Multiplicity of Singular Synchronous States in the Kuramoto Model of Coupled Oscillators

Maxim Komarov and Arkady Pikovsky

Department of Physics and Astronomy, University of Potsdam, Karl-Liebknecht-Strasse 24, D-14476 Potsdam, Germany and Department of Control Theory, Nizhny Novgorod State University, Gagarin Avenue 23, 606950 Nizhny Novgorod, Russia

(Received 9 August 2013; revised manuscript received 18 September 2013; published 15 November 2013)

We study the Kuramoto model of globally coupled oscillators with a biharmonic coupling function. We develop an analytic self-consistency approach to find stationary synchronous states in the thermodynamic limit and demonstrate that there is a huge multiplicity of such states, which differ microscopically in the distributions of locked phases. These synchronous regimes already exist prior to the linear instability transition of the fully asynchronous state. In the presence of white Gaussian noise, the multiplicity is lifted, but the dependence of the order parameters on coupling constants remains nontrivial.

DOI: 10.1103/PhysRevLett.111.204101 PACS numbers: 05.45.Xt, 05.45.−a

Since its introduction almost 40 years ago, the Kuramoto model of globally coupled oscillators [1] has been established as a standard model describing synchronization transitions in large populations of coupled oscillators. Similar to the Ising model in the theory of phase transitions, the Kuramoto model captures essential features of synchronization, observed in many physical systems, e.g., in Josephson junctions [2], atomic recoil lasers [3], spin-torque [4] and electrochemical [5] oscillators, as well as in a more interdisciplinary context, like for applauding persons in a large audience [6] and for pedestrians on footbridges [7]. For other examples, see Ref. [8].

The general Kuramoto model is formulated as a system of differential equations for the phases ϕ_k of N oscillators having natural frequencies ω_k, which are coupled globally:

$$\dot{\phi}_k = \omega_k + \frac{1}{N}\sum_{j=1}^{N}\Gamma(\phi_j - \phi_k). \quad (1)$$

The simplest and most studied case is that of sinusoidal coupling $\Gamma(\psi) = \varepsilon \sin\psi$. Here, the original analysis by Kuramoto [1] and its subsequent extensions [9,10] revealed a clear picture of the transition in the thermodynamic limit $N \to \infty$. For symmetric one-hump frequency distributions $g(\omega)$, there exists a critical coupling ε_c depending on $g_{\max}$, at which the synchronization sets in, and the order parameter (the mean field) grows $\sim(\varepsilon - \varepsilon_c)^{1/2}$. The situation is much less trivial for more general coupling functions Γ. For example, if both the first and the second harmonics are present [9,11,12], the transition may have a different scaling of the order parameter $\sim(\varepsilon - \varepsilon_c)$.

In this Letter, we report on rather surprising findings in the Kuramoto model (1) with a general biharmonic coupling function

$$\Gamma(\psi) = \varepsilon \sin(\psi) + \gamma \sin(2\psi) \quad (2)$$

and a unimodal distribution of frequencies, making this case distinct both from a particular problem with the second harmonics only [13] and from the situations where the second harmonics is considered perturbatively [9,11,12]. We show that (i) there exist synchronous regimes prior to the stability threshold of the desynchronized state, (ii) these regimes have order parameters that can take values anywhere in the range $(0, R_{\max}]$ for some $R_{\max} < 1$, (iii) there is a huge multiplicity of these states for fixed coupling parameters, and we estimate their number as growing exponentially with N, and (iv) when a small noise is added, the multiplicity is lifted, but a nontrivial synchronous regime coexists with the stable asynchrony.

Before proceeding with the analysis, we give three examples of realistic physical systems where the second harmonics term is strong or even dominating. The first example is the classical Huygens setup with pendulum clocks suspended on a common beam. Here, the horizontal displacement of the beam leads to the first harmonics coupling $\sim\varepsilon$, while the vertical mode produces the second harmonics term $\sim\gamma$ [14]. Another example is recently experimentally realized φ Josephson junctions [15], where the dynamics of a single element in the array is governed by a double-well energy potential. Therefore, one can expect strong effects caused by the second harmonics in the interaction. Third, in experiments with globally coupled electrochemical oscillators [16], a pronounced second harmonics has been observed in the coupling function inferred from experimental data.

Our approach is based on self-consistency equations for the order parameters, like in Refs. [1,13]. We start with introducing the two relevant order parameters according to $R_m e^{i\Theta_m} = N^{-1}\sum_k e^{im\phi_k}$ and rewrite Eq. (1) as

$$\dot{\varphi} = \omega + \varepsilon R_1 \sin(\Theta_1 - \varphi) + \gamma R_2 \sin(\Theta_2 - 2\varphi). \quad (3)$$

We consider the thermodynamic limit and assume the distribution of frequencies $g(\omega)$ to be symmetric; without loss of generality, we can set the central frequency to zero. Then, due to the symmetry of the coupling function and of the distribution, stationary solutions can be chosen with $\Theta_1 = \Theta_2 = 0$. Introducing the conditional distribution of the phases at a given frequency as $\rho(\varphi|\omega)$, we can represent the order parameters $R_{1,2}$ as

$$R_m = \iint d\varphi d\omega g(\omega)\rho(\varphi|\omega)\cos m\varphi, \qquad m = 1, 2. \quad (4)$$

To close these equations, we have to find $\rho(\varphi|\omega)$ using Eq. (3). All the phases can be separated in the rotating ones (if $|\omega|$ is large) and locked ones (small $|\omega|$). For rotating phases, the stationary distribution density is inversely proportional to the phase velocity $\rho_r(\varphi|\omega) = C|\omega - \varepsilon R_1 \sin(\varphi) - \gamma R_2 \sin(2\varphi)|^{-1}$, where C is the normalization constant. The locked phases satisfy the equation $\omega = \varepsilon R_1 \sin\varphi + \gamma R_2 \sin 2\varphi$. It is convenient to introduce $\cos\theta = \gamma R_2/R$, $\sin\theta = \varepsilon R_1/R$, $R = \sqrt{\gamma^2 R_2^2 + \varepsilon^2 R_1^2}$, and $x = \omega/R$, so that this equation takes the form $x = y(\theta, \varphi) = \sin\theta \sin\varphi + \cos\theta \sin 2\varphi$. In the following analysis, for the sake of brevity of presentation, we restrict ourselves to the case $R_{1,2} > 0$, $0 \le \theta \le \pi/2$; this implies a restriction on the possible range of parameters ε, γ, but all interesting effects are present. When finding φ as a function of x, we have to satisfy additionally the stability condition $(\partial/\partial\varphi)y(\theta, \varphi) > 0$ that follows from Eq. (3). The stable branches are clear from Fig. 1. For $\tan\theta > 2$, there is only one stable branch $\varphi = \Phi_1(x, \theta)$ in the range $-\varphi_1 < \varphi < \varphi_1$, $-x_1 < x < x_1$, where $\varphi_1 = \arccos[(-\sin\theta + \sqrt{\sin^2\theta + 32\cos^2\theta})/8\cos\theta]$ and $x_1 = y(\theta, \varphi_1)$ [Fig. 1(b)]. For $\tan\theta < 2$, there is an additional stable branch $\varphi = \Phi_2(x, \theta)$ with $\pi - \varphi_2 < \varphi < \pi + \varphi_2$, $-x_2 < x < x_2$, where $\varphi_2 = \arccos[(\sin\theta + \sqrt{\sin^2\theta + 32\cos^2\theta})/8\cos\theta]$ and $x_2 = -y(\theta, \varphi_2)$ [Fig. 1(a)].

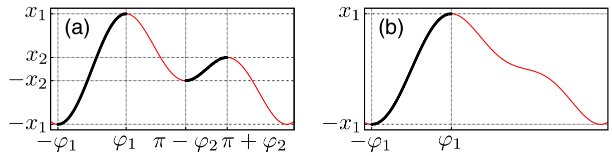

FIG. 1 (color online). Sketch showing stable phase branches (black bold line) vs frequency $x = \omega/R$.

Locked phases occupy these stable branches; thus, for the distribution $\rho_l(\varphi|\omega)$, we get

$$\rho_l(\varphi|\omega) = \begin{cases} [1 - S(\omega)]\delta[\varphi - \Phi_1(x, \theta)] + S(\omega)\delta[\varphi - \Phi_2(x, \theta)] & \text{for } |x| < x_2 \\ \delta[\varphi - \Phi_1(x, a)] & \text{for } x_2 < |x| < x_1. \end{cases} \quad (5)$$

Here, $0 \le S(\omega) \le 1$ is an indicator function describing the distribution over the branches; its dependence on ω is arbitrary. Because this function enters in the integral (4) only, it is an arbitrary integrable function with finite variation; i.e., it can be extremely nonsmooth. This is already an indication on the multiplicity of synchronous states (already mentioned in Ref. [13] for $\varepsilon = 0$), to be discussed in more detail below. Substituting distribution (5) in Eq. (4), we can represent the order parameters $R_{1,2}$ as functions of R, θ. We introduce

$$F_m(R, \theta) = \int_{-\pi}^{\pi} d\varphi \cos m\varphi \Big[A(\varphi) g(Ry) \frac{\partial y}{\partial \varphi} + \int_{|x|>x_1} dx C(x, \theta)|x - y(\theta, \varphi)|^{-1} \Big], \quad (6)$$

where the indicator function $A(\varphi)$ is $A(\varphi) = 1 - S(y)$ for $|\varphi| < \varphi_3$, $A(\varphi) = S(y)$ for $|\varphi - \pi| < \varphi_2$, $A(\varphi) = 1$ for $\varphi_3 < |\varphi| < \varphi_1$, and $A(\varphi) = 0$ otherwise. Here, φ_3 satisfies $y(\theta, \varphi_3) = y(-\theta, \varphi_2)$. The normalization constant is determined from $\int d\varphi C(x, \theta)|x - y|^{-1} = g(Rx)$. In terms of these integrals, we can represent the order parameters and the coupling constants parametrically, as

$$R_{1,2} = RF_{1,2}(R, \theta), \qquad \varepsilon = \frac{\sin\theta}{F_1(R, \theta)}, \qquad \gamma = \frac{\cos\theta}{F_2(R, \theta)}. \quad (7)$$

Relations (6) and (7) solve the problem of finding the stationary order parameters in an analytic form, for any indicator function $S(\omega)$. In Figs. 2–4, we illustrate the solutions for the simplest case, where $S(\omega) = \sigma$ is a constant, and for the Gaussian distribution of frequencies $g(\omega) = (2\pi)^{-1/2}\exp(-\omega^2/2)$.

We start with $\sigma = 0$ (so that all the phases are on one stable branch). Setting in Eqs. (6) and (7) $R \to 0^+$ and varying θ, we find a curve on the plane of parameters (ε, γ) where the order parameters $R_{1,2}$ vanish (line L_2 in Fig. 2). Between curves L_1 and L_2, there are two solutions. We also show curve L_3 corresponding to the parameter value $\tan\theta = 2$, which separates the two-branch [Fig. 1(a)] and the one-branch [Fig. 1(b)] situations (marked as C and B, correspondingly). Below L_3, there is a solution with $S(\omega) = 0$ only; above it, a multiplicity due to the arbitrariness of the indicator function $S(\omega)$ occurs. We also depict curves corresponding to synchronous solutions with $R_{1,2} = 0$ at fixed values of σ; to the right of these curves, synchronous states with corresponding values of σ exist.

We illustrate different synchronous regimes as functions of coupling parameters (ε, γ) in Figs. 3 and 4. Figure 3 shows the dependence of synchronous states on the coupling parameter ε, for fixed $\gamma = 0.85\gamma_{\text{lin}}$ (horizontal arrow in Fig. 2). Here, the synchrony arises at different values of ε for different σ, and immediately beyond the threshold, multiple synchrony states are possible. With a further increase of ε, when the line L_3 is crossed, multiplicity disappears. A different situation is shown in Fig. 4, where we increase γ at fixed $\varepsilon = 0.9\varepsilon_{\text{lin}}$ (vertical arrow in Fig. 2).

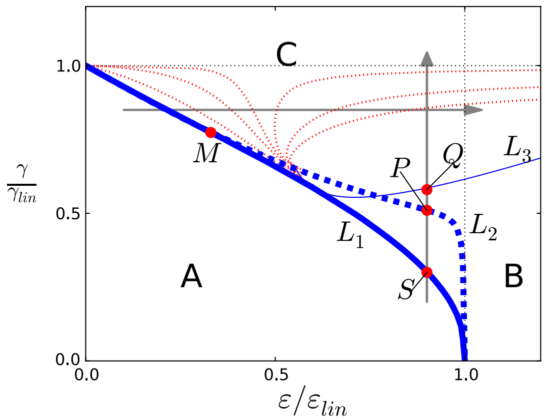

FIG. 2 (color online). Diagram of different synchronous states in dependence on parameters (ε, γ) resulting from from the analytical solution of Eqs. (6) and (7). The bold (blue) line L_1 represents the border of synchronous states; the bold dashed (blue) line L_2 shows where the order parameters vanish; when L_1 and L_2 split, there are two solutions (stable and unstable) with nonzero $R_{1,2}$ and the transition to synchrony is hard (see the region between points S and P in Fig. 4); when L_1 and L_2 coincide (above point M), there is a soft transition to synchrony (see Fig. 3). Above the solid (blue) line L_3 (drawn from the condition $\tan\theta = 2$), multiplicity of synchronous states occurs (beyond point Q in Fig. 4). The dotted (red) lines represent the onset of synchrony for $\sigma = 0.2$, 0.4, 0.5, 0.6, 0.8, 1 (from left to right). Arrows show routes depicted in Figs. 3 and 4; the dotted black lines are linear stability borders of asynchronous states. A, no synchronous states; B, single synchronous state; and C, multiple synchronous states.

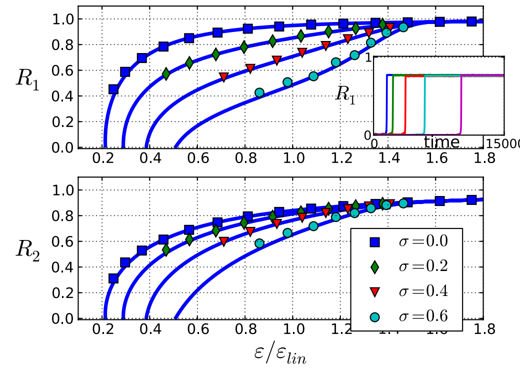

FIG. 3 (color online). Dependence of the order parameters on coupling ε for $\gamma = 0.85\gamma_{\rm lin}$ (curves). Markers are results of direct simulation of a population of $N = 2 \times 10^4$ oscillators. Different curves correspond to values of σ, as depicted in the panel. For $\varepsilon \gtrsim 1.6\varepsilon_{\rm lin}$, the solution is unique; for smaller ε, there are multiple states appearing at different critical couplings. The inset shows the time evolution of the order parameter R_1 in direct simulations of an ensemble (1) for $\gamma = 0.85\gamma_{\rm lin}$, $\varepsilon = 0.6\varepsilon_{\rm lin}$, and different N: from left to right, $N = 5 \times 10^4$, 10^5, 2×10^5, 5×10^5, 10^6.

Now, synchrony sets on at $\tan\theta > 2$, so that a unique synchronous solution appears and remains unique until the border of multiplicity $\tan\theta = 2$ (point Q) is crossed. Multiple solutions exist for all larger values of γ. A special solution with $\sigma = 0.5$ appears at the linear threshold $\gamma = \gamma_{\rm lin}$: this regime, because of symmetry, contains only the second order parameter ($R_1 = 0$) and corresponds to the bifurcation from the asynchronous state, as described in Ref. [9].

Unfortunately, we cannot analyze analytically the stability of the constructed solutions. The only analytic results we can rely on are stability calculations of the asynchronous state $R_{1,2} = 0$, yielding instability for $\varepsilon > \varepsilon_{\rm lin}$ or $\gamma > \gamma_{\rm lin}$, and neutral stability due to a continuous spectrum otherwise [9,12,17]. Thus, we checked for stability via direct numerical simulation of the large ensembles. They follow the theoretically predicted curves, as the markers show in Figs. 3 and 4. At low values of $R_{1,2}$, these solutions, however, can hardly be confirmed due to finite-size effects, to be considered elsewhere [18]. Remarkably, the linearly neutrally stable asynchronous state, in the region beyond the curve L_2, where synchronous solutions also exist, appears in simulations to be only *metastable*. After a transient, which becomes longer for very large ensembles, the ensemble evolves abruptly to one of the synchronous states; we illustrate this in the inset of Fig. 3. Thus, although the curves in Fig. 4 look like those for a standard hysteretic transition, they are not: at point P, the zero equilibrium does not become linearly unstable; instead, it remains linearly neutrally stable in the thermodynamic limit but is metastable due to finite-size effects. This neutral stability or metastability also allows synchronous states to appear with arbitrary small amplitudes $R_{1,2}$ (see in Fig. 2 curve L_2 and corresponding curves for different

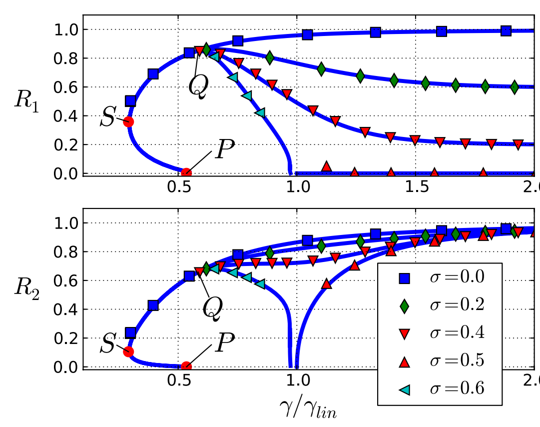

FIG. 4 (color online). Same as Fig. 3, but for $\varepsilon = 0.9\varepsilon_{\rm lin}$. For $\gamma \lesssim 0.6\gamma_{\rm lin}$, there is a unique synchrony state; for larger couplings, multiplicity is observed. Point S denotes a saddle-node bifurcation at which coherent states appear (curve L_1 in Fig. 2). At point P, the unstable branch of the coherent solution vanishes (curve L_2 in Fig. 2). Between points S and P, a finite perturbation of the incoherent state is needed to come to a synchronous regime. Point Q, the onset of multiplicity, corresponds to curve L_3 in Fig. 2.

values of σ, which occupy the whole region on this diagram, and also Fig. 3). Therefore, the points in Fig. 3 where $R_{1,2}$ vanish do not correspond to a usual bifurcation from an equilibrium and cannot be described as the points where the incoherent state becomes linearly unstable. This is due to the singularity of the appearing states: as one can see from Eq. (5), the density includes a combination of delta functions for any small $R_{1,2}$, similar to the Van Kampen modes in plasmas [19], while in the stability analysis [9], one operates with modes which apparently cannot describe constructed singular solutions.

Next, we discuss the issue of multiplicity. As mentioned above, in the thermodynamic limit, any indicator function can be used, so that to a macrostate with given ε, γ, $R_{1,2}$ belong to many microstates with different redistributions between the stable branches. We illustrate this in Fig. 5. In fact, we can easily estimate the rate of the multiplicity. We can view the locked oscillators in the bistability range as uncoupled spins. Assuming for simplicity that the phases of two branches differ by π, we conclude that the order parameter R_2 does not depend on the "spin orientation," i.e., on which branch they are sitting, while R_1 can be interpreted as a "magnetization." Then, finding that the number of different microstates reduces to a textbook problem of calculating the entropy $\mathcal{S}(R_1)$ with a constant magnetization for noninteracting spins. Thus, the number of microstates grows exponentially with the number of locked oscillators in the range of bistability N_{bist}, which is less than N but is a macroscopic quantity for $R_{1,2}$ that is not too small, as $\sim \exp[\mathcal{S}(R_1)N_{\mathrm{bist}}]$.

Remarkably, both the multiplicity and the singularity are lifted by adding a small Gaussian white noise to the phase dynamics, replacing Eq. (1) with the Langevin model

$$\dot{\phi}_k = \omega_k + \frac{1}{N}\sum_{j=1}^{N}\Gamma(\phi_j - \phi_k) + \sqrt{D}\xi_k(t). \qquad (8)$$

Now, in the thermodynamic limit for each ω, the distribution (5) is no more an arbitrary combination of delta functions but a smooth unique distribution density. Thus, the multiplicity is removed. Because this distribution is nonsingular, it belongs to the class of functions used in the linear stability and in the bifurcation analysis [9,12,17]. We confirm this in Fig. 6, where we show the dependence of the order parameters on coupling, for two different levels of noise. Here, we used both the extension of the self-consistent analysis as above, where in the integral Eq. (4) the distribution density is taken as the solution of the Fokker-Planck equation corresponding to Langevin model (8) (details will be presented elsewhere [18]), and the results of direct simulations of the density evolution equation of the whole system using mode expansion. While the former method gives stable and unstable solutions, the latter one selects the stable branches only. Comparing with Figs. 3 and 4, we see that both multiplicity and singularity are lifted. Because the stability of the incoherent state is no more neutrally but asymptotically stable [17], a hysteretic transition to synchrony is of a standard type accompanying a subcritical bifurcation.

In conclusion, we have described nontrivial synchronous states that appear in the Kuramoto model with a biharmonic coupling function. Because of a possibility to have two stable branches of phase-locked oscillators, one observes a multiplicity of microstates. On the macrolevel, this multiplicity manifests itself as the existence of a whole range of possible order parameters for given coupling constants. Remarkably, these states appear prior to the linear instability of the asynchronous regime and are not captured by the linear stability analysis. When a noise is added, the multiplicity is lifted, but the transition to synchrony may become hysteretic, with a region of bistability synchrony-asynchrony. We stress that the self-consistent approach developed allows us to find stationary synchronous states but does not deliver their stability properties. To check for stability, we performed simulations with large ensembles in the noise-free case, which revealed the metastability of the asynchronous state and simulated the

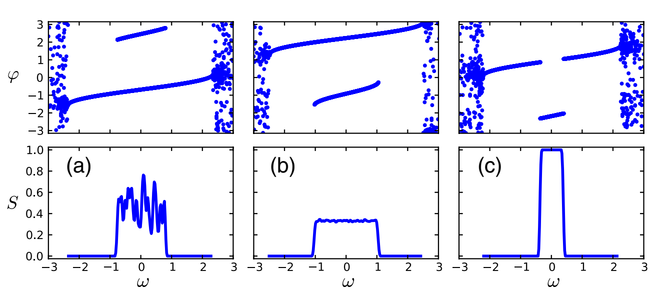

FIG. 5 (color online). Illustration of multiplicity of states ($\varepsilon = \gamma = 1.25\varepsilon_{\mathrm{lin}}$, $N = 2 \times 10^4$). In all cases, one can see two stable branches of locked phases and the corresponding coarse-grained indicator function $S(\omega)$. In (a), the redistribution between branches is random; in (b) and (c), we kept $S(\omega)$ to be constant with values 0.33 and 1.

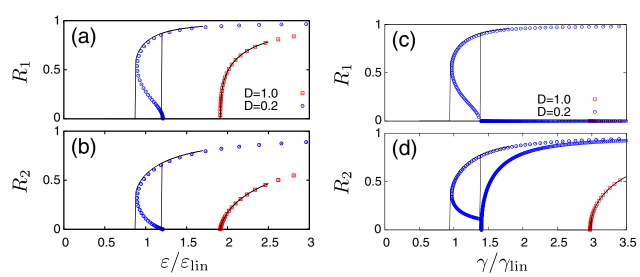

FIG. 6 (color online). Dependence of order parameters on the couplings ε, γ, (a),(b) for $\gamma = 0.8\gamma_{\mathrm{lin}}$ and for (c),(d) $\varepsilon = 0.75\varepsilon_{\mathrm{lin}}$ in the presence of noise [Eq. (8)]. Markers are values obtained from self-consistent analysis; the bold black line is a result of simulation of the density evolution, yielding dynamically stable branches. The branch in (c) and (d) corresponding to the symmetric state $R_1 = 0$, $R_2 > 0$ is unstable dynamically for $D = 0.2$ but stable for $D = 1$.

evolution of the probability density in the presence of noise. More details about the regimes in the full range of parameters, and on the limit of small noise, will be presented elsewhere [18].

M. K. thanks the Alexander von Humboldt Foundation for support. We acknowledge useful discussions with M. Rosenblum, I. Kiss, and R. Toenjes.

[1] Y. Kuramoto, in *International Symposium on Mathematical Problems in Theoretical Physics*, edited by H. Araki, Springer Lecture Notes in Physics Vol. 39 (Springer, New York, 1975), p. 420; *Chemical Oscillations, Waves and Turbulence* (Springer, Berlin, 1984).
[2] K. Wiesenfeld and J. W. Swift, Phys. Rev. E **51**, 1020 (1995); K. Wiesenfeld, P. Colet, and S. H. Strogatz, Phys. Rev. Lett. **76**, 404 (1996); K. Wiesenfeld, P. Colet, and S. H. Strogatz, Phys. Rev. E **57**, 1563 (1998).
[3] J. Javaloyes, M. Perrin, and A. Politi, Phys. Rev. E **78**, 011108 (2008).
[4] J. Grollier, V. Cros, and A. Fert, Phys. Rev. B **73**, 060409 (R) (2006); B. Georges, J. Grollier, V. Cros, and A. Fert, Appl. Phys. Lett. **92**, 232504 (2008).
[5] I. Kiss, Y. Zhai, and J. Hudson, Science **296**, 1676 (2002).
[6] Z. Néda, E. Ravasz, T. Vicsek, Y. Brechet, and A. L. Barabási, Phys. Rev. E **61**, 6987 (2000).
[7] B. Eckhardt, E. Ott, S. H. Strogatz, D. M. Abrams, and A. McRobie, Phys. Rev. E **75**, 021110 (2007).
[8] J. A. Acebrón, L. L. Bonilla, C. J. P. Vicente, F. Ritort, and R. Spigler, Rev. Mod. Phys. **77**, 137 (2005).
[9] J. D. Crawford, Phys. Rev. Lett. **74**, 4341 (1995); J. D. Crawford and K. T. R. Davies, Physica (Amsterdam) **125D**, 1 (1999).
[10] E. Ott and T. M. Antonsen, Chaos **18**, 037113 (2008); **19**, 023117 (2009).
[11] H. Daido, Physica (Amsterdam) **91D**, 24 (1996).
[12] H. Chiba and I. Nishikawa, Chaos **21**, 043103 (2011).
[13] P. S. Skardal, E. Ott, and J. G. Restrepo, Phys. Rev. E **84**, 036208 (2011).
[14] K. Czolczyński, P. Perlikowski, A. Stefański, and T. Kapitaniak, Commun. Nonlinear Sci. Numer. Simul. **18**, 386 (2013).
[15] E. Goldobin, D. Koelle, R. Kleiner, and R. G. Mints, Phys. Rev. Lett. **107**, 227001 (2011); E. Goldobin, R. Kleiner, D. Koelle, and R. G. Mints, Phys. Rev. Lett. **111**, 057004 (2013).
[16] I. Z. Kiss, Y. Zhai, and J. L. Hudson, Phys. Rev. Lett. **94**, 248301 (2005); Prog. Theor. Phys. Suppl. **161**, 99 (2006).
[17] S. H. Strogatz and R. E. Mirollo, J. Stat. Phys. **63**, 613 (1991).
[18] M. Komarov, V. Vlasov, and A. Pikovsky (unpublished).
[19] N. G. Van Kampen, Physica (Amsterdam) **21**, 949 (1955).